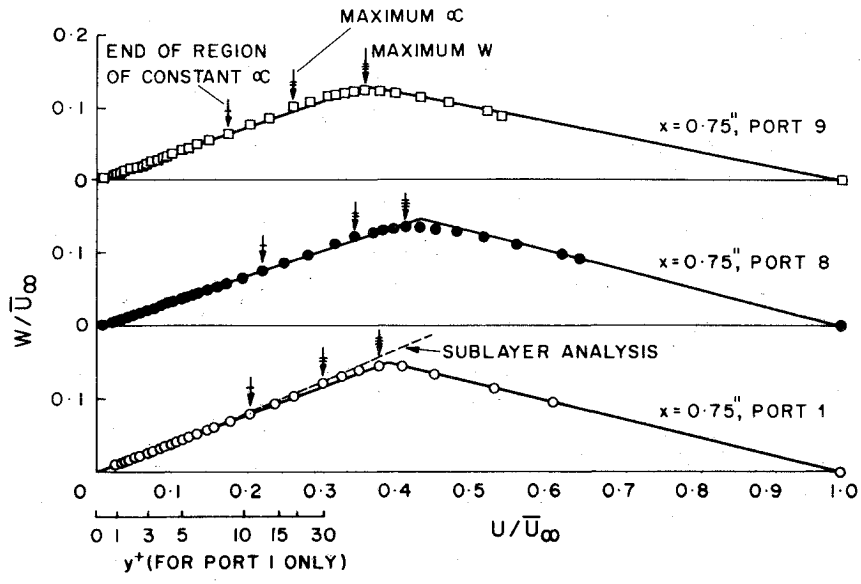

Fig. 2 Polar plots of mean velocity profile (ports 1, 8, and 9).

analysis because the estimates of the wall pressure gradients at these locations were considered to be more accurate and reliable. Some typical values of change of crossflow angle $\Delta\alpha$ predicted by the analysis are compared with the experimental data in Refs. 7 and 8. The analysis predicts conservative results (overestimates), the overestimation increasing with distance from the wall. This is to be expected as the effect of the wall static pressure field decreases with distance from the wall. The overestimation is also seen in the predicted profile shapes which have a slight curvature upward (Fig. 2). Within the limitations of the analysis, the estimated decrease of crossflow angle compares favorably with the measured value.

Conclusion

This Note clearly points to the importance of and difficulties in obtaining reliable measurements and reliable flow conditions near the wall of skewed flows. It suggests that even slight lateral adverse pressure gradients could be initiating reversal of the crossflow, with the first sign of this reversal being the collateral layer and decreasing flow angles near the wall. With these considerations of the near-wall flowfield, it is conceivable that in the absence of the small local transverse pressure gradients close to the wall, the skewing of the flow could have been much more pronounced practically down to the wall (limited only by the resolution of the sensor), implying a noncollateral flowfield consistent with the equations of motion in the neighborhood of the wall.

Acknowledgment

This work formed a part of the investigation carried out by the author at the Aerospace Engineering Department of the University of Maryland. The author wishes to thank W.L. Melnik and A.E. Winkelmann.

References

[1] East, J.L., Jr. and Pierce, F.J., "Explicit Numerical Solution of the Three-Dimensional Incompressible Turbulent Boundary Layer," *AIAA Journal,* Vol. 10, Sept. 1972, pp. 1216-1223.

[2] Pierce, F.J. and East, J.L., Jr., "Near-Wall Collateral Flow in Three-Dimensional Boundary Layers," *AIAA Journal,* Vol. 10, March 1972, pp. 334-336.

[3] Pierce, F.J. and Zimmerman, B.B., "Wall Shear Stress Inference from Two- and Three-Dimensional Turbulent Boundary Layer Velocity Profiles," *Journal of Fluids Engineering, Transactions of ASME,* Ser. I, Vol. 95, 1973, pp. 61-67.

[4] Nash, J.F. and Patel, V.C., *Three-Dimensional Turbulent Boundary Layers,* SBC Technical Books, Atlanta, Ga., 1972.

[5] Rogers, B.K. and Head, M.R., "Measurement of Three-Dimensional Boundary Layers," *The Aeronautical Journal of the Royal Aeronautical Society,* Vol. 73, 1969, pp. 796-798.

[6] Vermeulen, A.J., "Measurements of Three-Dimensional Turbulent Boundary Layers," Ph.D. Dissertation, Univ. of Cambridge, 1971.

[7] Hebbar, K.S., "An Experimental Investigation of the Near-Wall Region of a Three-Dimensional Incompressible Turbulent Boundary Layer Relaxing in a Zero Pressure Gradient," Ph.D. Dissertation, Univ. of Maryland, 1976.

[8] Hebbar, K.S. and Melnik, W.L., "Measurements in the Near-Wall Region of a Relaxing Three-Dimensional Low Speed Turbulent Air Boundary Layer," Dept. of Aerospace Engineering, Univ. of Maryland, TR No. AE-76-1, July 1976.

[9] Klinksiek, W.F. and Pierce, F.J., "Simultaneous Lateral Skewing in a Three-Dimensional Turbulent Boundary Layer Flow," *Journal of Basic Engineering, Transactions of ASME,* Ser. D, Vol. 92, 1970, pp. 83-92.

Ice-Crystal/Shock-Layer Interaction in Hypersonic Flight

T. C. Lin* and N. A. Thyson†
Avco Systems Division, Wilmington, Mass.

WHEN a re-entry vehicle flying through the Earth's atmosphere traverses a cloud, raindrops or ice crystals may strike the nosetip at high speed, causing serious damage to the heatshield. The shock layer surrounding the vehicle tends to shatter, decelerate, and melt the incoming debris and hence acts as a shield against the erosive environment. In order to make accurate predictions of the nosetip erosion, one must first understand the kinematics of these ambient particles and their thermal environment. The analytical results presented here are focused on the dynamics of ice crystals in the shock layer, although the formulation can be extended to particles other than ice.

Heating Environment

Previous investigations concerning the kinematics of particles in the shock layer include either vaporization or melting processes.[1,2] In the latter case, it is assumed that the

Received March 15, 1977; revision received July 12, 1977.
Index categories: Multiphase Flows; Supersonic and Hypersonic Flow.

*Presently Technical Staff Member, The Aerospace Corporation. Member AIAA.
†Department Head. Member AIAA.

aerodynamic force is sufficient to remove the liquid melted layer immediately. So far, only Wu[3] has considered the so-called blockage effect. His analysis follows Bethe and Adams' work,[4] which originally was designed for glassy materials. We shall adopt a mathematical model for the heating environment which includes three layers, namely, the air boundary layer and the liquid and thermal layers in the ice crystal. The solutions for these three layers are coupled.

Heat Conduction in the Ice Particle

The unsteady one-dimensional heat-conduction equation for a spherical ice particle is

$$\frac{\partial T}{\partial t} = \frac{\sigma}{r^2}\frac{\partial}{\partial r}\left(r^2\frac{\partial T}{\partial r}\right) \tag{1}$$

where T is temperature, σ is the thermal diffusivity, t is time, and r is the local body radius. The appropriate boundary and initial conditions are $T(t,a)=T_m$, $T(0,r)=T_0$, and $\partial T(t,0)/\partial r=0$, where T_m is the melting temperature and a is the particle radius. Then Eq. (1) has the solution

$$T=T_0+(T_m-T_0)\left[1+\frac{2a}{\pi r}\sum_{n=1}^{\infty}\frac{(-1)^n}{n}\times\sin\frac{n\pi r}{a}\exp\left(\frac{-\sigma n^2\pi^2 t}{a^2}\right)\right]$$

Air Boundary Layer

The heat transfer from an air boundary layer with mass injection at a stagnation point of a sphere can be correlated as[3]

$$\psi=(\dot{q}_0)_i/\dot{q}_0=1-0.98M^{0.34}B+9.24M^{0.71}B^2 \tag{2}$$

where $B=\dot{m}_i(H_s-H_i)/\dot{q}_0$, M is the ratio of molecular weights of air to injected vapor (H_2O), $\dot{m}_i$ is the rate of surface mass transfer, H_s and H_i are the total enthalpy at the boundary-layer edge and wall, respectively, ψ is the heating blockage parameter, and $\dot{q}_0$ and $(\dot{q}_0)_i$ are the laminar flow stagnation-point heat transfer without and with mass injection, respectively. Equation (2) agrees well with experimental data[5] and exact numerical solutions.[6]

Liquid Layer

The governing equations for the liquid layer on a spherical ice particle are

$$(\mu f''/\bar{\mu})_\eta + ff'' + \tfrac{1}{2}[\rho_e/\bar{\rho}-f'^2]=0 \tag{3a}$$

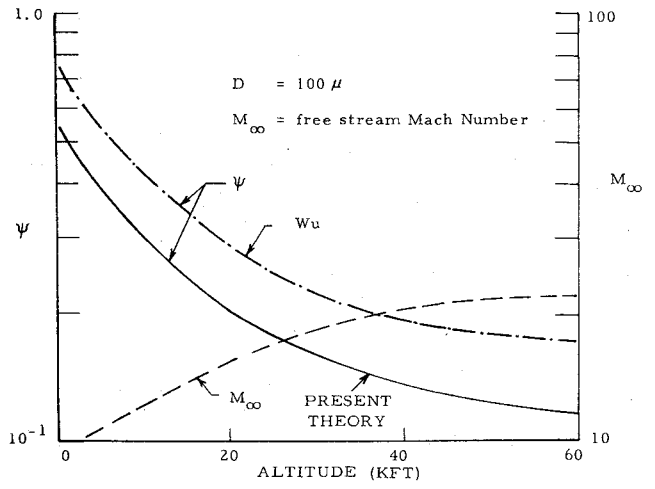

Fig. 1 Distribution of heating blockage parameter for a typical flight trajectory (spherical ice particle).

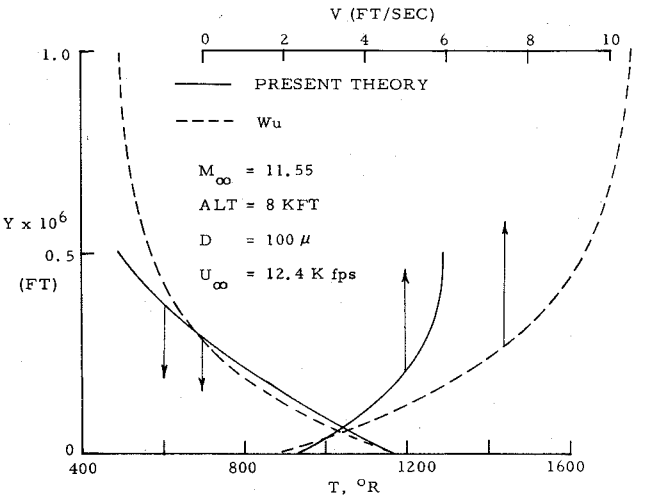

Fig. 2 Radial velocity and temperature profile on a spherical ice particle.

$$K\theta_{\eta\eta}/C_p\bar{\mu}+f\theta_\eta=0 \tag{3b}$$

where

$$\xi=\bar{\rho}\bar{\mu}\int_0^s u_e r^2\,ds, \qquad \eta=\frac{\bar{\rho}u_e}{\sqrt{2\xi}}ry$$

and where

$f'=u/u_e$ = velocity ratio
K = thermal conductivity
μ = viscosity
C_p = specific heat
ρ = density
$\theta=(T-T_m)/(T_i-T_m)$

and where $\bar{\rho}$ and $\bar{\mu}$ are the density and viscosity of water at 0°C, respectively. Subscript i refers to the conditions at the interface of liquid and air. The corresponding boundary conditions are

$$\eta=0,\ \theta=1,\ \theta_\eta=\psi\dot{q}_0 Pr^{1/3}E/[\mu_i(H_e-H_i)]$$

$$f_{\eta\eta}=\frac{\psi\dot{q}_0 E}{\mu_i(H_e-H_i)},\quad E=\left[\frac{\bar{\mu}}{2\bar{\rho}(du_e/ds)}\right]^{1/2}$$

and Pr = Prandtl number, H = total enthalpy, and $\eta=\eta_\delta$, $f_\eta=0$, $\theta=0$.

Since η_δ is also an unknown, one additional heat-balance equation is needed:

$$\psi\dot{q}_0=\dot{m}_m[\Delta h_f+h_T]+\dot{m}_i\Delta h_v+\left(K\frac{\partial T}{\partial r}\right)_{\text{ice}}$$

where $h_T=0.6\,C_p(T_i-T_m)$, $\dot{m}_i$, $\dot{m}_m$ = mass-transfer rate at $\eta=0$ and η_δ, and where Δh_f and Δh_v are the heat of fusion and vaporization, respectively. This expression for the heat-capacity term h_T follows Lees' analysis,[7] which includes convection as well as heat absorption by the melted layer. The $K(\partial T/\partial r)$ denotes the rate of heat conduction into the ice crystal.

The coupled boundary-value problem just outlined has been solved numerically by the method of quasilinearization.‡ The heating blockage parameter ψ is plotted in Fig. 1 for a typical flight trajectory with ballistic coefficient $\beta=2360$ psf. These results indicate that the heat-transfer shielding effect caused by mass injection significantly reduces ice-crystal

‡In the numerical example, $T_m=T_0$ is assumed in the ice crystal [see Eq. (1)].

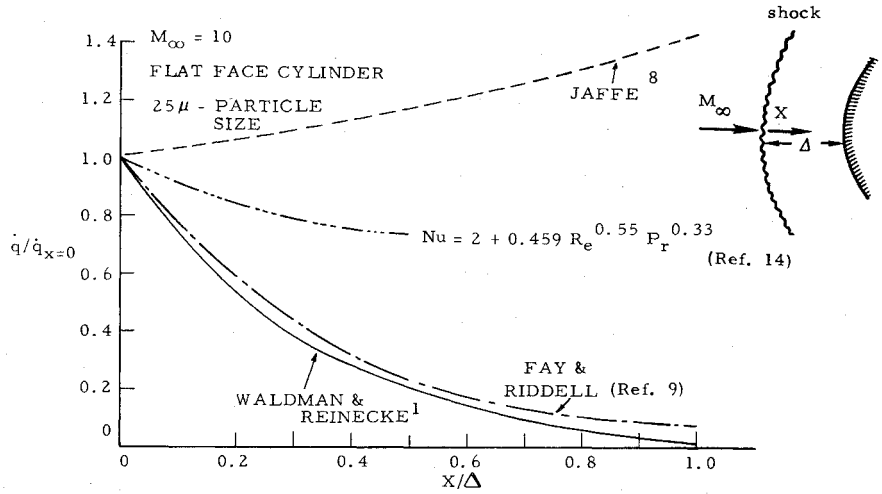

Fig. 3 Comparison of various heating models for melting of ice crystals: spherical ice particle.

melting in the shock layer. The liquid-layer velocity and temperature profiles are shown in Fig. 2. Comparison of our results with the approximate solution of Ref. 3 also is shown in Figs. 1 and 2. Wu's closed-form solution overpredicts the liquid-layer thickness.

In the existing literature, attention has been focused on obtaining closed-form solutions. However, there has been disagreement on the formulation of the heat transfer $\dot{q}_0$. For example, Jaffe[8] assumed a constant Nusselt number, i.e., $\dot{q}_0 \sim (Nu/2r)K\Delta T$, where Nu = Nusselt number = const, and $\Delta T = T_s - T_i$, whereas Waldman and Reinecke[1] employed the relation $\dot{q}_0 \sim (u/u_\infty)^3 r^{-1/2}$, where u = particle velocity, and u_∞ = freestream velocity. A comparison between these two approaches and a more exact heating model, that of Fay and Riddell,[9] is depicted in Fig. 3. Jaffe's formula[8] predicts that $\dot{q}_0$ increases as the melting ice particle traverses the shock layer (since r becomes smaller). Waldman and Reinecke's model[1] compares favorably with Fay and Riddell's solution.[9]

Kinematics of Ice Crystals in the Shock Layer

When ice crystals enter the shock layer, they will be decelerated, tumbled, heated, and melted away. The governing equations for the motion of one particle are

$$dx/dt = u, \qquad dy/dt = v \tag{4a}$$

$$m\,du/dt = -\tfrac{1}{2}\rho_g C_D A q(u - U_g) - \tfrac{1}{2}\rho_g C_L A q(v - V_g) \tag{4b}$$

$$m\,dv/dt = -\tfrac{1}{2}\rho_g C_D A q(v - V_g) - \tfrac{1}{2}\rho_g C_L A q(u - U_g) \tag{4c}$$

where u and v are velocity components in the x and y directions; C_D and C_L are the drag and lift coefficients, respectively; $q = [(u - U_g)^2 + (v - V_g)^2]^{1/2}$; and A is the particle projected surface area. The particle mass is given by $m = 4/3\,\rho\pi r^3$ for a spherical crystal.

We shall assume that the flowfield is not affected by the presence of the ice crystal. The distributions of gas velocity components U_g and V_g and density ρ_g are obtained from exact inviscid flow computations.[10] The drag and lift coefficients are determined by empirical fitting of the extensive experimental data compiled in Refs. 11 and 12.

To evaluate the mass loss caused by melting, we follow Waldman and Reinecke's formulation.[1] The average heating on a sphere is taken to be 53% of its stagnation-point value, and the laminar stagnation-point heat transfer without mass injection $\dot{q}_0$ is evaluated by Fay and Riddell's relation.[9] Equations (4) have been integrated numerically. The variation of the impact particle kinetic energy fraction at the stagnation point after passage through the shock layer on a flat-faced cylinder is shown in Fig. 4. The ambient particles have been taken to be cylinders at an angle of 60 deg to the flight direction and with a ratio of length to radius of 6. The results show that, for a body radius of 1 in., the shock layer will dissipate 22% of the initial particle energy of 200-μ-diam ice crystals and 80% for 50-μ-diam crystals at impact.

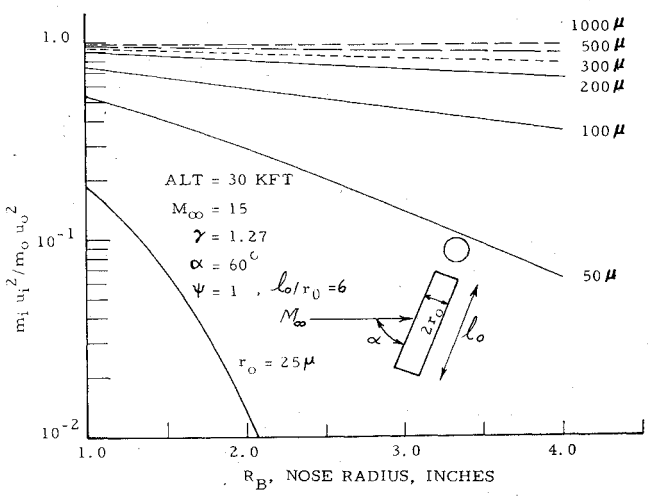

Fig. 4 Distribution of impact kinetic energy ratio at flat-face cylinder stagnation point as function of nosetip radius and particle size: cylindrical ice particle.

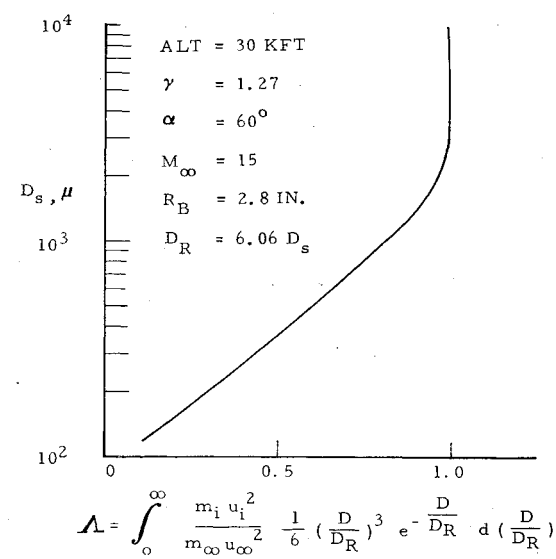

Fig. 5 Statistically average kinetic energy ratio at impact: cylindrical ice particle (flat-face cylinder stagnation point).

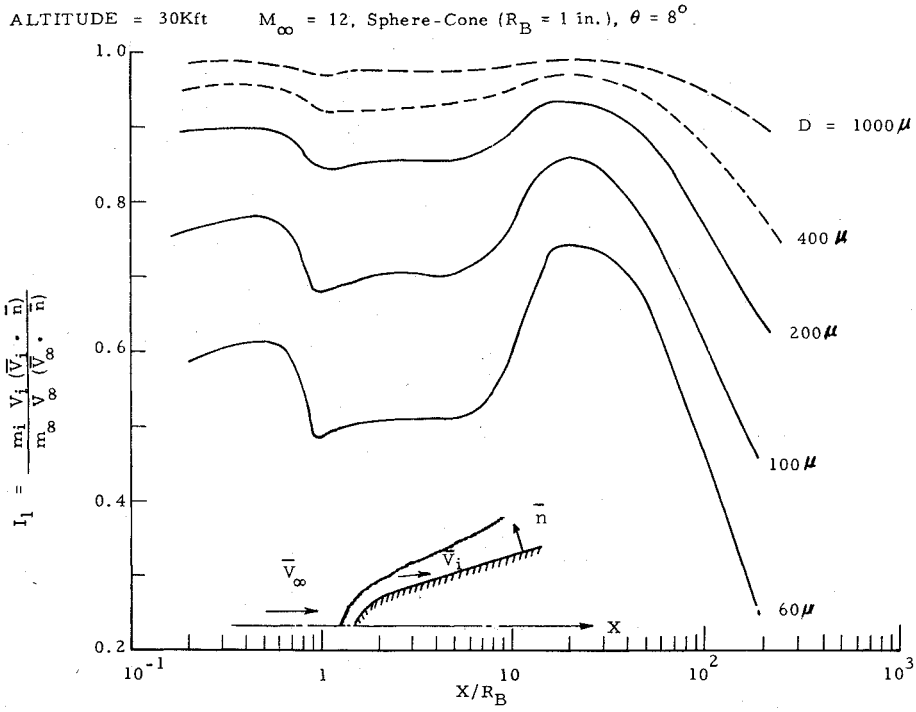

Fig. 6 Ice-crystal kinetic energy impact ratio on blunt cone: spherical ice particle.

The statistical particle size distribution function for ice crystals can be represented by an exponential relation.[1] The net kinetic energy impact fraction at the stagnation point then becomes

$$\Lambda = \int_0^\infty \frac{m_i u_i^2}{6 m_\infty u_\infty^2} \zeta^3 \exp(-\zeta) d\zeta, \quad \zeta = \frac{D}{6.06 D_S}$$

where m_∞ represents ambient particle mass, subscript i denotes conditions at impact, and D_S is a reference particle diameter.[1] Figure 5 shows the variation of Λ with D_S for a 2.8-in. body cylinder radius. Numerical results for spherical ice particle impact downstream of the stagnation region are shown in Fig. 6. Here we have considered a sphere-cone body geometry with a cone half-angle of 8 deg. For the larger ice particles, the trajectory deflection and slow-down attributable to shock layer effects is insignificant and can be neglected. For the smaller ice crystals ($D<200$ μ), the shock layer becomes an effective shielding mechanism in decelerating the particle. It is interesting to note that a minimum appears in $I_I = m_i V_i (\bar{V}_i \cdot \bar{n}) / m_\infty V_\infty (\bar{V}_\infty \cdot \bar{n})$ near the cone-sphere junction.§ Far downstream (e.g., $X/R_B > 25$), I_I starts to decrease due to the thickening of the shock layer. This behavior of I_I is associated principally with the increase in the particle deflection angle.

In Ref. 13, we have considered the questions of the spinning of ice particles, the effects of thermal shock, and the problem of high-temperature radiant energy transfer. It was concluded that the thermal shock effects and the tumbling of the cylindrical ice particles are not important because of the small-particle residence time. A large angular velocity is induced, however, which may cause the ice to crack or break up.

References

[1] Waldman, G. and Reinecke, W., "Particle Trajectory, Heating and Breakup in Hypersonic Shock Layers," *AIAA Journal*, Vol. 9, June 1971, pp. 1040-1048.

[2] Probstein, R. F. and Fassio, F., "Dusty Hypersonic Flows," *AIAA Journal*, Vol. 8, April 1970, pp. 772-779.

[3] Wu, P.K.S., "Advanced Reentry Aeromechanics," Physical Sciences, Inc., Wakefield, Mass., PSI-TR-10, Aug. 30, 1974.

[4] Bethe, H. A. and Adams, M. C., "A Theory for the Ablation of Glassy Materials," *Journal of the Aerospace Sciences*, Vol. 26, June 1959, pp. 321-358.

[5] Pappas, C. C. and Lee, G., "Heat Transfer on a Hypersonic Blunt Cone with Mass Addition," *AIAA Journal*, Vol. 8, May 1970, pp. 954-956.

[6] Lewis, C. H., Adams, J. C., and Gilley, G. E., "Effects of Mass Transfer and Chemical Nonequilibrium on Slender Blunted Cones," ARO, Inc., Tullahoma, Tenn., AEDC-TR-68-214, Nov. 1968.

[7] Lees, L., "Similarity Parameters for Surface Melting of a Blunt Nosed Body in a High Velocity Gas Stream," *ARS Journal*, Vol. 29, May 1959, pp. 345-354.

[8] Jaffe, N. A., "Droplet Dynamics in a Hypersonic Shock Layer," *AIAA Journal*, Vol. 11, Nov. 1973, pp. 1562-1564.

[9] Fay, J. A. and Riddell, F. R., "Theory of Stagnation Point Heat Transfer in Dissociated Air," *Journal of the Aerospace Sciences*, Vol. 25, Feb. 1958, p. 73.

[10] Liu, T. M., "3-D Inviscid Flow Analysis," Avco System Div., Wilmington, Mass., AVSD-0335-74-RR, Dec. 1974.

[11] Bailey, A. B. and Hiatt, J., "Free-Flight Measurements of Sphere Drag," ARO, Inc., Tullahoma, Tenn., AEDC-TR-70-291, March 1971.

[12] Hoerner, S. F., "Fluid Dynamic Drag," published by the author, 1958.

[13] Lin, T. C. and Thyson, N., "Investigations of Ice Crystals in the Shock Layer of a High Speed Vehicle," Avco Systems Div., Wilmington, Mass., Avco TR-K210-74-17, Sept. 1974.

[14] Carlson, D. J. and Hoglund, R. F., "Particle Drag and Heat Transfer in Rocket Nozzles," *AIAA Journal*, Vol. 12, Nov. 1963, pp. 1980-1984.

§Here I_I represents the shock-layer shielding effect on ice-crystal kinetic energy impact ratio.

Heat Transfer in Wall Jet Flows with Vectored Surface Mass Transfer

Rama Subba Reddy Gorla*
Cleveland State University, Cleveland, Ohio

Nomenclature

C_f = local skin friction coefficient
E = Eckert number $U^2/cp\ (T_w - T_\infty)$
f = nondimensional stream function

Received Feb. 14, 1977; revision received April 25, 1977.
Index categories: Boundary Layers and Convective Heat Transfer—Laminar; Thermal Control.

*Associate Professor, Department of Mechanical Engineering.